Contents lists available at ScienceDirect

Ceramics International

Selenization process in simple spray-coated CIGS film

Nandang Mufti [a,b,*], Atika Sari Puspita Dewi [a], Rosita Kartika Putri [a], Saparullah [a], Ahmad Taufiq [a,b], Sunaryono [a], Hadi Nur [c]

[a] Department of Physics, Faculty of Mathematics and Natural Sciences, Universitas Negeri Malang, Malang, 65145, Indonesia
[b] Centre of Advanced Material for Renewable Energy, Universitas Negeri Malang, Malang, 65145, Indonesia
[c] Centre for Sustainable Nanomaterials, Ibnu Sina Institute for Scientific and Industrial Research, Universiti Teknologi Malaysia, Johor Bahru, Malaysia

ARTICLE INFO

ABSTRACT

The synthesis process to produce a decent thin-film CIGS layer with simple, easy, and low-cost are essential factors in CIGS solar cell technology. This study synthesized a thin layer of CIGS by a simple spray coating method and selenization process. The temperature substrate and distance between the nozzle and target are controlled to provide an even thickness coating. A one-stage selenization was carried out with temperature variations of 350, 400, and 500 °C and a three-stage selenization process as the comparison was made at 400 and 520 °C. The surface morphology, thickness, and optical properties of CIGS films were investigated as a function of the temperature of selenization. The complete CIGS solar cell prototype consists of a window, buffer, and CIGS absorber layer. The buffer layer used is ZnS deposited by the chemical bath deposition method, while the window layer of ZnO is deposited by the spin coating method. The SEM characterization showed a thinner layer of CIGS as temperature, and the heating rate of the selenization increased. The increasing selenization temperature also affects the Selenium deficiency that causes low Ga/(In + Ga) content and increases the bandgap energy. By the grain growth model and the kinetic study yielded estimated activation energy, which one step selenization of the process is higher than the three steps of the selenization process. PV82QJC8Y.

1. Introduction

Solar energy is among the most widely used energy sources globally. The average energy radiated by the Sun to the Earth's surface is about 184 W/m^2, which is 5000 times the global energy consumption [1]. Some technology has been developed to exploit solar energy, such as solar cells. Three generations of solar cells have developed until today. First-generation solar cells are based on silicon wafers such as polycrystalline and monocrystalline silicon. This type of solar cell is the most available in the market and has been widely used. The second generation of solar cells adopted thin-film technology, including amorphous silicon, CdTe, and CIGS, accounting for about 20% market share. On the other side, the third generation of solar cells such as CZTS, Perovskite, DSSC, Quantum Dot Solar cell, etc. is researched on the laboratory scale in industries and universities, which is why most of this generation is still not commercially available [2].

The second generation of solar cells based on Chalcopyrite materials such as CIGS (Copper Indium Gallium Selenium) is a promising alternative to silicon solar cells due to their high absorption coefficient and tunable bandgap, which maximizes the light absorption [3]. The efficiency of CIGS solar cells on a lab-scale is reported to be relatively high, up to 20% [4–6]. Additionally, CIGS can be a candidate for new solar cells which has the potential for comercial productiondue to the photodegradation stability and relatively low-cost compared to CdTe and amorphous silicon [7,8].

Generally, CIGS solar cells' structure consists of a conductive substrate (SLG/Molybdenum), an absorber layer (CIGS), a buffer layer (CdS), and a window layer (ZnO) [6,7]. Each layer has an essential role in the solar cells' overall performance. The conductive substrate is the "container" for coating materials as well as wiring for conducting direct electricity. As an absorber layer, p-type semiconductor CIGS functions as the main component that absorbs sunlight [9]. The window layer widely used in CIGS solar cells is a material with a wide-bandgap such as ZnO, which is an n-type semiconductor [10]. Heterojunction between CIGS and ZnO causes mismatch lattice and a fairly large bandgap difference between the two. So that an additional layer is needed to bridge the difference, it is known as a buffer layer. Cadmium Sulfide (CdS) is a well-established material and is commonly used as a buffer layer in CIGS
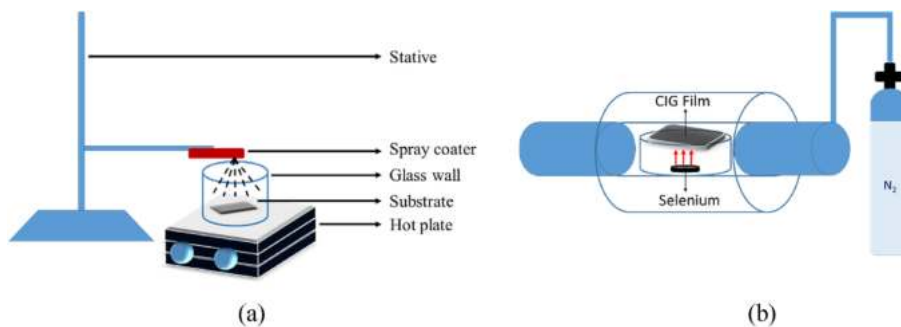
Fig. 1. Set up of the (a) spray coater and (b) selenization of CIGS in a vacuum furnace.

[11]. Recently, the use of cadmium is decreasing as it is toxic to the environment. Thus, we need other materials that are more environmentally friendly and do not reduce the function and effectiveness of the buffer layer on the CIGS solar cell. Such a material could be Zinc Sulfide (ZnS), which has a 3,2–3,6 eV bandgap [12] that can reduce the current losses in the CdS due to the narrow bandgap [13].

Although CIGS solar cells have a great potential for commercial production, high-efficiency CIGS are mostly produced by vacuum deposition methods such as sputtering and co-evaporation [14,15]. Besides requiring high technology investment and strict environmental control, this method requires relatively expensive costs. Zhang et al., in 2016 have developed solution-based CIGS, which can be deposited by simple spin-coating using hydrazine solution and other metal precursors which are annealed under inert conditions [16]. However, hydrazine is a toxic material for humans and the environment [17]. Solution-based CIGS synthesis has been conducted in previous studies, which have developed a solution-based synthesis of CIGS by hot injection method without hydrazine and deposited by knife coating and spin coating [18, 19]. However, the results of deposition by this method are heterogeneous, too thick, and the output produced is unstable. As an alternative to this problem, deposition using the spray-coating method for Cu, In, and Ga materials (CIG ink) is carried out to produce a thinner film. Selenization was used in this study as a substitute for hydrazine, which serves to carry Se so that it can bind to other elements (Cu, In, Ga).

The selenization process contributes to t he ratio of Ga/(In + Ga), which will affect the CIGS solar cells' optical properties and efficiency [20]. Several parameters must be considered when conducting selenization, including the selenization temperature, heating rate, soaking time, and the number of selenization stapes. The number of selenization steps influences the film morphology, as one-step selenization tends to crack in high temperatures [21], while multi-selenization of CIGS film is less prone to cracking and has a thinner film. The research that examines the deposition of CIGS followed by selenization has been reported by several researchers with kinds of methods such as doctor blade, inkjet printing, and spray coating [22–24]. What these studies have in common is the use of non-vacuum deposition followed by one-step selenization with several parameters as independent variables. However, no study compares one-step to multi-step selenization towards CIGS film deposited by spray coating. In this study, the effect of one-step selenization was investigated at temperatures of 350, 400, and 500 °C. In comparison, three steps of selenization at 400 °C and 520 °C were carried out to determine the effect on the morphology, and properties of the CIGS film.

2. Experimental details

The synthesis was started by dissolving three mmol Cu(acac)$_2$, 2.1 mmol In(acac)$_2$, and 0.9 mmol Ga(acac)2 in 15 ml of oleylamine at 285 °C with a holding time of 30 min. During this process, the ink was stirred while nitrogen gas was flowing. The ink was cooled at room temperature and stored in a vacuum chamber. The ink was deposited by a simple spray coating method. The ITO substrate was placed on a hot plate at 300 °C. Spray coating was carried out for 60 s at a constant volume. Heating at a constant temperature for 1 h was done to dry off the CIG layer on the substrate. The set-up of the spray-coating equipment is shown in Fig. 1 (a).

After the spray coating, the selenation process was conducted to add selenium to the CIG film to form a CIGS layer. Selenium was evaporated in a vacuum furnace until it adhered to the CIG film, as shown in Fig. 1 (b). In this selenation stage, various temperature treatments were carried out. In the first treatment, the CIGS film was single-stepped at temperatures of 350, 400, and 500 °C. For comparison, three stages of selenization were carried out at 400 and 520 °C. The process of the
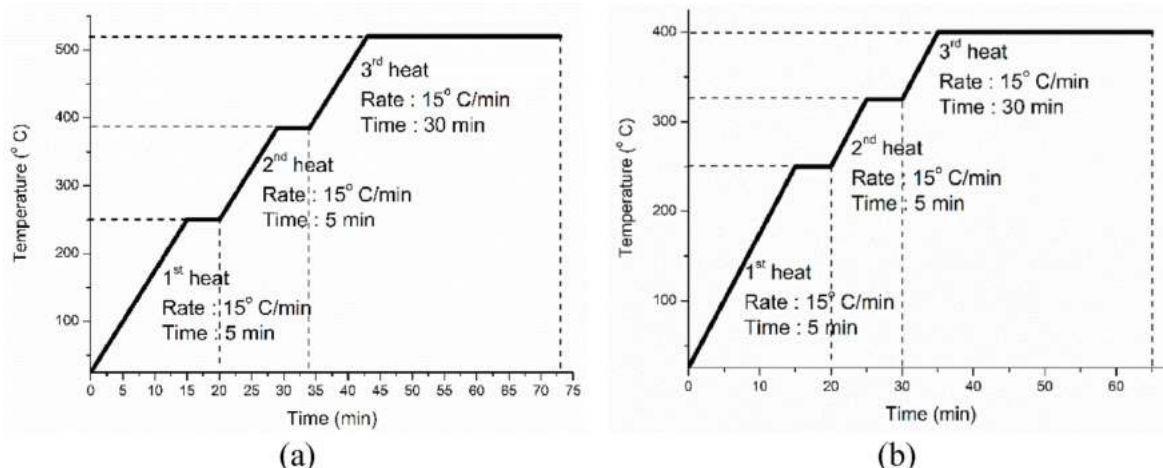

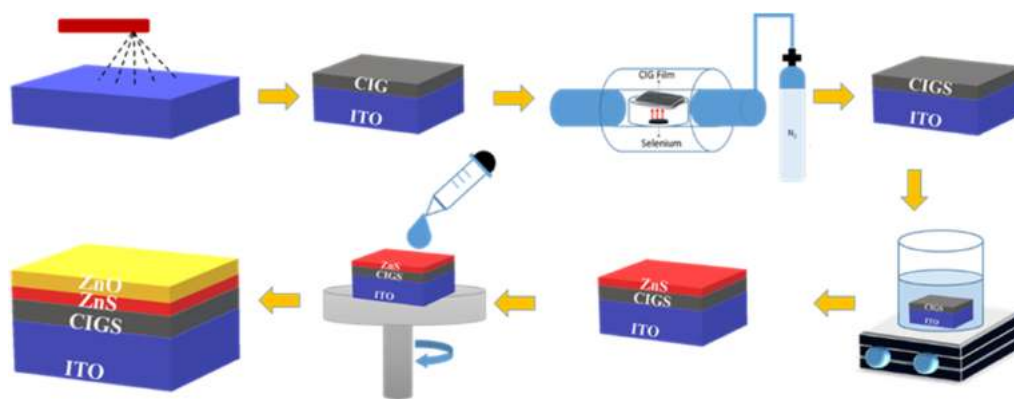Fig. 2. Three steps of selenization process (a) 520 and (b) 400 °C.

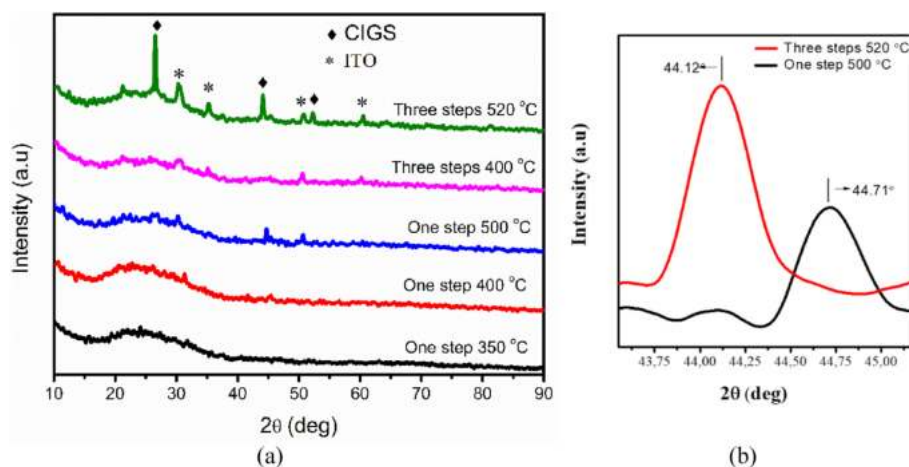**Fig. 3.** CIGS/ZnS/ZnO film deposition stages.

Fig. 4. (a) Diffraction pattern of CIGS with one and three steps selenization process at varying temperature (b) The comparison peak of 220/204 with one-step selenization at 500 °C and three-step selenization at 520 °C.

three-step selenization is shown in Fig. 2(a) and (b). The final product of this stage is called the CIGS film.

The zinc sulfide (ZnS) layer as the buffer layer was deposited using the chemical bath deposition (CBD) method. A total of 0.019 M zinc sulfate ($ZnSO_4.7H_2O$) in 50 ml deionized water, 0.17 M thiourea (CH_4N_2S) in 50 ml deionized water, and 1.92 M ammonia (NH_3) 25% in 43.5 mL of deionized water was stirred at 80 °C for 15 min. ZnS layer was deposited on a glass substrate by soaking ITO/CIGS film in the solution for 12 min.

The window layer used in this study is ZnO nanoparticles deposited by the spin coating method. In this method, 0.22 g of zinc acetate (Zn $(CH_3COO)_2 \cdot 2H_2O$) were dissolved in 5 mL of ethanol. The solution was stirred for 45 min at 70 °C. Then, 0.06 mL of monoethanolamine (MEA) was mixed into the solution and then stirred for 3 h. The final solution was dripped onto the substrate in a spin coater at a speed of 2000 rpm. The coating was carried out three times and annealed at 250 °C for 1 h. The fabrication of the CIGS solar cell was done by layering ZnS and ZnO on top of the CIGS layer, by chemical bath deposition and spin coating methods. The order of deposition of each layer is shown in Fig. 3.

The surface morphology, thickness, and porosity analysis were obtained by Field Emission Scanning Microscopy (SEM), Merk FEI, Type: Inspect-S50. The composition of the elements for each film was detected by Energy Dispersive X-Ray Spectroscopy (EDX). X-Ray Diffraction (XRD) peaks patterns were obtained by Cu-k_α Merk PanAnalytical, Type E'xpert Pro.

3. Results and discussion

CIGS, as an absorber layer, is coated with a two-step method, CIG coating with a spray coating method, and selenization to add the selenium element. The effect of selenation on the XRD diffraction pattern was investigated by varying the one-step selenization at 350, 400, and 500 °C and three steps selenization at 400 and 520 °C, with a soaking time of 30 min for each sample. In the selenization process, the selenium will evaporate and stick to the top of the CIG layer after reaching the melting point. After reaching a temperature above 350 °C (confirmed by SEM results), the Se layer will bind to In and enter the Cu–Ga layer. Then, Se can bind to Cu_2In and Cu_3Ga and react to In_2Se_3, Cu_2Se, and Cu_3Se_2 from CIGS [24].

Fig. 4 shows the diffraction pattern of each sample with variations in temperature during the selenization process. In samples selenized at temperatures of 350 and 400 °C, no peaks were detected, as shown in Fig. 4.1(a) and (b). This corresponds to the previous research by Huang et al., reporting that chalcopyrite crystals in CIGS thin films are formed at temperatures above 500 °C for 20 min of soaking time [25].

Both one-step selenization and three-step selenization of the sample selenized under 500 °C tended to have an amorphous diffraction pattern, which can be seen in Fig. 4 (a) and (b), where there is no visible CIGS peak. This indicates that the selenium layer is amorphous. Similarly, previous research by Liu et al. and Moon et al. revealed that the selenium deposited by the selenization technique is amorphous [26, 27] and that selenium heated under 500 °C has not cooperated with In or Ga, which is why the XRD detects no peak.

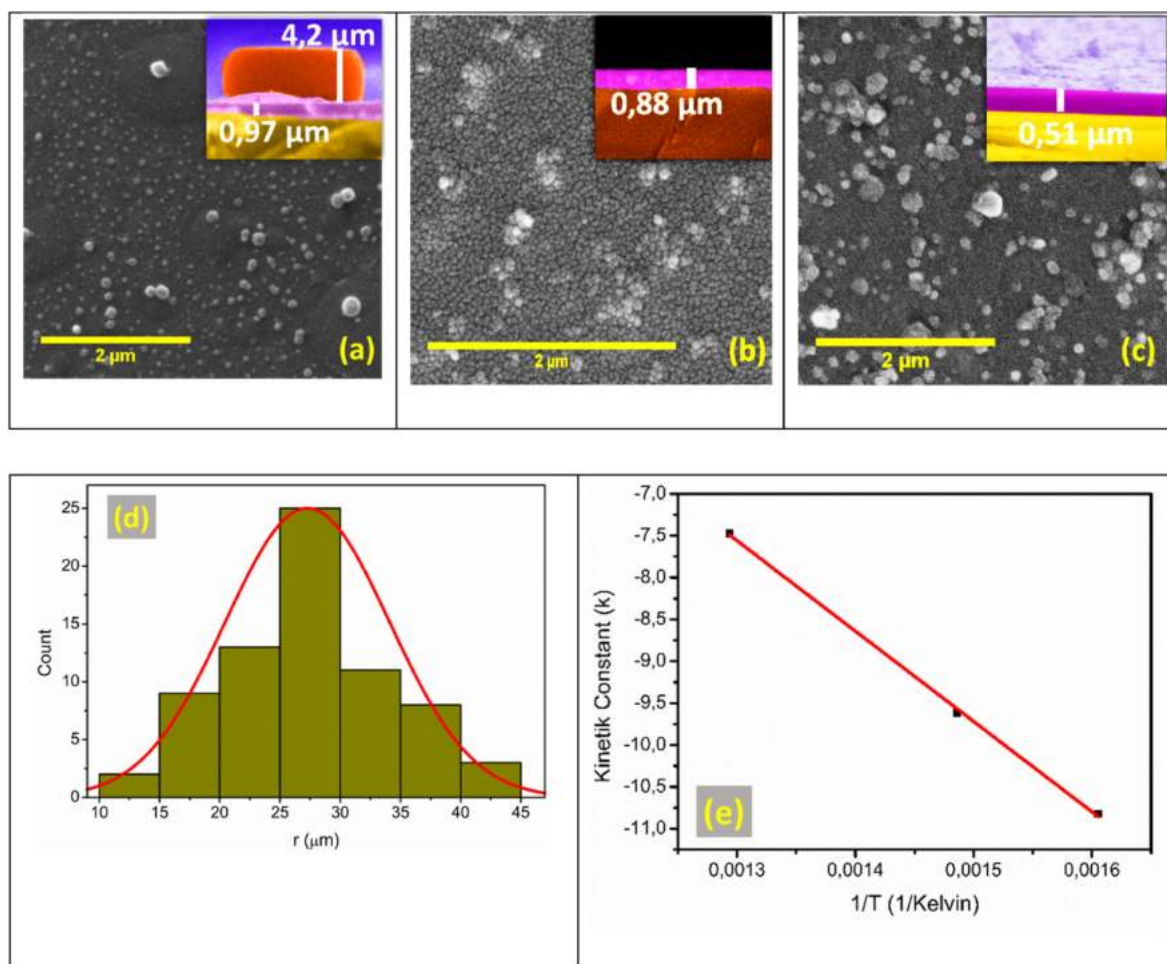The three-steps selenized sample at 520 °C in Fig. 4 (e) shows several

Fig. 5. Surface morphology, cross-section, and porosity of CIGS with one-step selenization at (a) 350, (b) 400, (c) 500 °C, and (d) normal distribution curve of the radian of particles shows that the hyperbolic curve n = 2, and (e) Arrhenius plot is the temperature function depends on the constant kinetic k from the r-value based on the hyperbolic growth curve (d).

CIGS higher intensity peaks at 26.42° (112), 44.20° (220/204), and 52.42° (312/116). These peaks correspond to the 35–1102. JCPDS chalcopyrite peaks [28]. The (112) sharp peak shows the absense of secondary phase that demonstrated good crystallinity and high purity of selenized CIGS [29]. Other samples with one-step selenization at 500 °C, as shown in Fig. 4 (a), have several peaks on the (220/204) plane with shallow intensity and are dominated by the ITO substrate. The low intensity of the peak cause by the temperature which is not high enough for the chalcopyrite crystal to grow. Further, there is peak shifting at (220/204), compared to the three-steps selenized sample at 520 °C, as seen in Fig. 4 (b). This shifting is caused by the unbound In compound within the chemical reaction during selenization. In this peak, only CuGaSe is fully formed. This compound was also detected by the peak shifting to the right, as reported by Mousavi et al. The (220/204) peak for the three-steps selenized film at 520 °C is detected at 44,12°. In contrast, the one-step selenized film at 500 °C is detected at 44,71°. Based on this result, the three-step selenization process with a heating rate of 15 °C/min with some rem requires more time so the crystal can optimally grow compared to the one-step seenization process.

The SEM analysis shows the surface morphology and the cross-section of CIGS film selenized in one step at 350, 400, and 500 °C, as shown in Fig. 5. Fig. 5 (a) shows that some Se particles with a thickness of 4.2 μm have not been fused at a selenation temperature of 350 °C. The heating rate during selenation at 350 °C is 16.25 °C/min. The CIG layer, which was selenized in one step at a temperature of 400 °C and 500 °C using heating rates of 18.75 °C/min and 23.75 °C/min produced a CIGS

layer of 0.88 μm and 0.51 μm thickness, as seen in Fig. 5 (b)–(c), respectively. The layer with a thickness below 1 μm is known as an ultrathin film. The performance produced by the ultrathin film is not much different from the absorber layer with a thickness of more than 1 μm [30].

The growth distribution of one-step selenized CIGS grain size at 400 °C has a normal fitting that shows that one-step selenized CIGS particles are spread evenly, as presented in Fig. 5 (d). The grain-size distribution of the other samples shows similar behavior. This parabolic growth is the common equation that explains grain growth particles mathematically formulated by different approaches [31].

$$r^n - r_0^n = kt \tag{1}$$

The kinetic constant is in accordance with the parabolic growth law. The equation from this curve explains that the growth of particle sizes depends on the function of temperature, as shown in equation (1). In the equation, $r_0 = 0$ represents the nanoparticle precursors and n = 2 due to the parabolic function, as shown by the particle growth.

$$\ln k = \frac{-Ea}{RT} + \ln A \tag{2}$$

$$y = mx + c \tag{3}$$

The Arrhenius plot, as shown in Fig. 5 (e), is based on equation (2), with T in Kelvin. This equation is equal to the linear equation (3), where the x-axis is 1/T in the Arrhenius plot, and the activation energy Ea is equal to the gradient m. Therefore, the activation energy is the
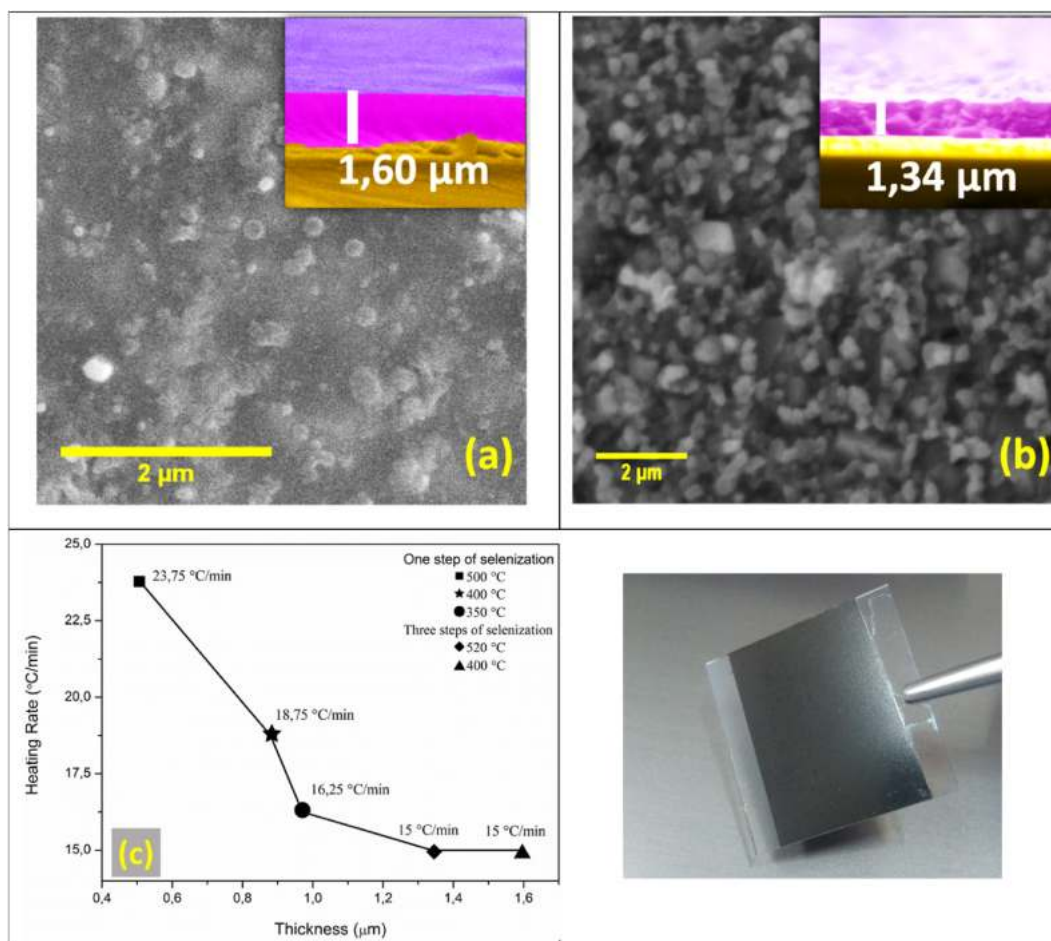
Fig. 6. SEM cross-section and porosity of CIGS with a three-stage selenation process at (a) 400 and (b) 520 °C, and (c) the relationship between the heating rate and the CIGS layer thickness.

multiplication between R (gas constant = 8.314 J mol^{-1} K^{-1}) and the gradient. Based on the Arrhenius plot, the activation energy is 89. 715 J mol^{-1} K^{-1} and is the minimum energy the precursors need to react and form CIGS in one-step selenization. Similarly, the activation energy of three-steps selenized CIGS at 400 and 520 °C is 49,340 J mol^{-1} K^{-1}.

The activation energy is the minimum that should be fulfilled for the atoms or molecules in the chemical system to react and form the final product [32]. The activation energy is also considered a dividing line between two energy states, the precursors and the product. A chemical reaction will occur if the dividing line is exceeded. The energy source, in this case, is temperature. The higher the selenization temperature, the higher the kinetic energy of the atoms in a reaction. This causes a bigger collisions frequency between atoms, making it easier for the atoms to exceed the activation energy [33]. This happens in both one-step and three-step selenization processes. In the three-step selenization process, the activation energy is lower than the three-step selenization process. This is the consequence of the enhanced particles growth, although the

samples are in accordance with the normal growth principle. The particles' size increases with the temperature increment, showing that the higher the kinetic constant, the bigger the change of kinetic energy towards temperature, and the higher the activation energy. In the three-step selenization process, the kinetic constant is higher than the one-step selenization process, but the constant kinetic alteration at 400 and 520 °C is not more significant than the one-step selenization process, meaning that the activation energy is lower. In other words, the three-step selenization process will make the CIGS particles to be growing better than the one-step selenization process.

One-step selenization obtained a thicker CIGS layer compared to a three-step, as shown in Fig. 6 (a) and (b). Samples selected at 400 and 520 °C had thicknesses of 1.60 and 1.34 μm, respectively These two samples are accelerated with the same heating rate, which is 15 °C/min in each step. The thicker layer is caused by a lower Se loss, compared to single-step selenation. This result echoes the previous research by Bi et al. and Chen et al., where even a single-stage selenation with a high heating rate can cause cracking and peeling of the CIGS coating [34,35].

The effect of heating rate and thickness of the resulting CIGS is presented in Fig. 6 (c). Based on the graph, it is clear that the higher the heating rate, the thinner the resulting layer. This is because the faster the heating occurs, the more material evaporates and escapes from the film. In the three steps, despite using the same heating rate, the thickness is different due to the different final holding temperatures used. Se loss will still occur even in a three-stage process. The samples that were selenized at a temperature of 520 °C produced a thinner layer than the samples selenized at 400 °C. Generally, the thickness produced by the spray coating method and selenized produces a thinner layer when

Table 1
The porosity of each film with the variation of selenization.

Variation of selenization temperature	Porosity (%)
One-step selenization	
350 °C	78.47
400 °C	68.32
500 °C	72.15
Three-steps selenization	
400 °C	63.14
520 °C	76.03

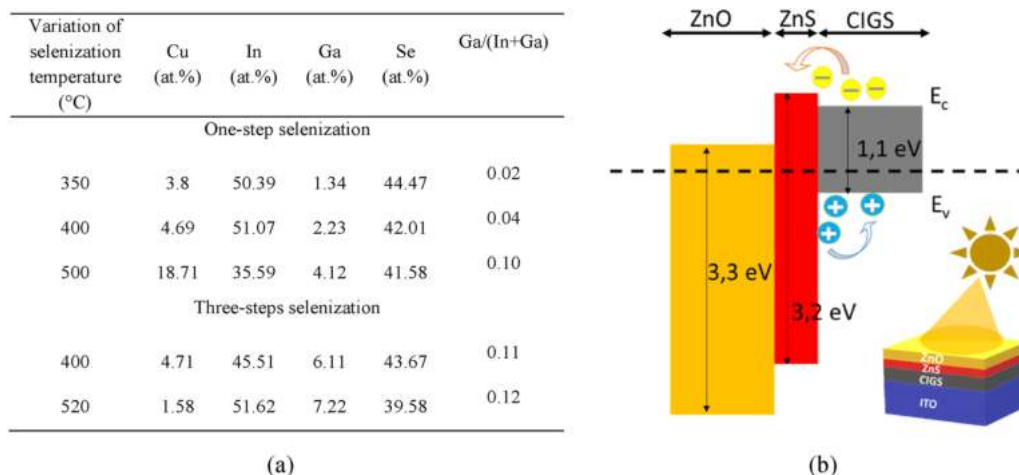| Variation of selenization temperature (°C)	Cu (at.%)	In (at.%)	Ga (at.%)	Se (at.%)	Ga/(In+Ga)
One-step selenization					
350	3.8	50.39	1.34	44.47	0.02
400	4.69	51.07	2.23	42.01	0.04
500	18.71	35.59	4.12	41.58	0.10
Three-steps selenization					
400	4.71	45.51	6.11	43.67	0.11
520	1.58	51.62	7.22	39.58	0.12

(a)

(b)

Fig. 7. (a) Mechanism of electron-hole movement in CIGS solar cells and (b) Chemical composition measured by EDX characterization of CIGS absorber layer with various selenization treatments.

compared to the knife coating or spin coating method, which was carried out as a preliminary study [14,15].

The selenization aims to regulate the composition, and selenium will bind to In and Ga to form $InSe_2$ and $GaSe_2$ when selenized. Energy level $InSe_2$ is lower than $GaSe_2$. Thus, when more Ga binds to the Se, the conduction band will shift upwards, which causes the bandgap to become wider.

The SEM analysis showed different morphologies. The surface morphology is characterized by the Origin software to determine the porosity. The porosity of each sample is shown in Table 1. The porosity of the CIGS film layer is the substrate layer that is not coated with CIGS material, or the area of the substrate coated with CIGS is thinner than the surrounding area [36].

Table 1 shows that the porosity increases with the selenization temperature in both the one-step and three-step methods. The increase in porosity with temperature rise was due to the increase in CIGS nucleation, as shown in the SEM results. Crystal growth was increasing (confirmed by XRD), accompanied by increasing grain boundaries. This increase in grain boundaries causes the pores to become wider. The growth of nucleation in CIGS was also reported by Lin et al. [37]. The porosity of the film heated at 350 °C was 78.47%, which is higher than the porosity of the film selenized at a higher temperature. This is due to a large number of unmelted selenium layers. Thus, the area around the selenium becomes lower and is detected as pores.

The CIGS film, which was one-step selenized at a temperature of 400 and 500 °C, showed an increasing porosity, namely 68.32% and 72.15%, respectively. Per the previously stated definition, higher porosity indicates more porosity compared to the material covered by the CIGS material. In the same vein, such a condition occurs in the three-step selenization at 400 °C and 520 °C porosity to 63.14% and 76.03%, respectively. This increase in porosity has a positive impact as it reduces the effect of light reflection to maximize photon absorption. Solar cells with 60% porosity can reduce reflections up to 7.3% [38].

Based on the results of EDX characterization, the ratio of Ga/(In + Ga) content for each sample was obtained, as shown in Fig. 7 (a). Based on these results, the ratio of Ga/(In + Ga) content is much smaller than the results obtained by Wu et al. This results in a decreasing CIGS bandgap, thereby increasing the possibility of recombination in the CIGS layer. Regarding this, research by Choubrac et al. [39] has shown that the bandgap value is not suitable for CIGS results in a decrease in the overall performance of CIGS solar cells. Similar results were obtained by Wu et al. The best performance of CIGS solar cells is obtained when the Ga/(In + Ga) ratio is ~0.3, and the bandgap is ~1.14 eV [21]. This result is in agreement with the SEM results, which showed that the sample selenized at 350 °C with a lot of unmelted selenium resulting in a

suitable CIGS composition is not achieved.

When light hits the sample, CIGS acts as an absorber layer with a bandgap of 1.1–1.68 eV [40] absorbing most wavelengths of light passing by and releasing electrons and holes. The free electrons will then move to the ZnS layer 3.2 eV–3.6 eV [41] and ZnO 3.3 eV–3.6 eV [42,43] before finally flowing into the circuit of Fig. 7(b). However, when the ratio of Ga/(In + Ga) is under 0.3, conductive band shifting will be closer to the fermy energy, so that the electron will not move to the n-type semiconductor but merge with the hole, increasing the recombination probability. On the other hand, when the Ga/(In + Ga) ratio increases, the conduction band will be shifted away from the Fermi energy, reducing the possibility of recombination [44,45]. Consequently, it allows for an increase in the value of V_{OC}. This finding is in line with the research by Paul et al., which shows that, when the ratio of Ga/(In + Ga) is lower or higher than 0.3, the value of V_{OC} [46,47] will decrease.

4. Conclusions

The crystallinity of CIGS indicated by the results of XRD data analysis showed an increase in the selenization temperature. The thickness of the CIGS layer decreases with an increase in selenization temperature, which also increases the percentage of the resulting film's porosity that improves the light reflection effect. The ratio of Ga/(In + Ga) increases with the rise in temperature, which is due to the growing number of materials bonded to the CIGS film. The increase in the Ga/(In + Ga) ratio can also increase V_{OC} in solar cells. The particle growth in the one-step selenization process delivers higher activation energy than the three steps of selenization, indicating that the CIGS particles' size is easier to form by the three-step selenization.

Declaration of competing interest

The authors declare that they have no known competing financial interests or personal relationships that could have appeared to influence the work reported in this paper.

Acknowledgments

References

[1] BP, Statistical Review of World Energy, 2014. Available at: https://www.bp.com/en/global/corporate/energy-economics/statistical-review-of-world-energy/downloads.html.

[2] T. Zhang, et al., A review of the energy performance and life-cycle assessment of building-integrated photovoltaic (BIPV) systems, Energies 11 (11) (2018) 3157, https://doi.org/10.3390/en11113157. Nov.

[3] Y.-C. Wang, et al., A critical review on flexible Cu(In, Ga)Se2 (CIGS) solar cells, *Mater. Chem. Phys.*, Agu 234 (2019) 329–344, https://doi.org/10.1016/j.matchemphys.2019.04.066, 2019.

[4] H. Heriche, et al., High-efficiency CIGS solar cells with optimization of layers thickness and doping, *Optik*, Des 127 (24) (2016) 11751–11757, https://doi.org/10.1016/j.ijleo.2016.09.071, 2016.

[5] N. Mufti, et al., Review of CIGS-based solar cells manufacturing by structural engineering, Sol. Energy 207 (Sep. 2020) 1146–1157, https://doi.org/10.1016/j.solener.2020.07.065, hal.

[6] L. Yan, et al., Extending absorption of near-infrared wavelength range for high efficiency CIGS solar cell via adjusting energy band, Curr. Appl. Phys. 18 (4) (Apr. 2018) 484–490, https://doi.org/10.1016/j.cap.2017.12.015.

[7] M.M.A. Moon, et al., Comparative study of the second generation a-si:H, CdTe, and CIGS thin-film solar cells, Adv. Mater. Res. 1154 (2019) 102–111. https://doi.org/10.4028/www.scientific.net/AMR.1154.102.

[8] J.-M. Delgado-Sanchez, Luminescent solar concentrators: photo-stability analysis and long-term perspectives, Sol. Energy Mater. Sol. Cells 202 (2019), 110134, https://doi.org/10.1016/j.solmat.2019.110134. Nov.

[9] R.L. Garris, et al., Electrical characterization and comparison of CIGS solar cells made with different structures and fabrication techniques, Sol. Energy Mater. Sol. Cells 174 (2018) 77–83, https://doi.org/10.1016/j.solmat.2017.08.027. Jan.

[10] I. Gharibshahian, et al., Potential efficiency improvement of Cu (In, Ga) Se2 thin-film solar cells by the window layer optimization, Thin Solid Films 655 (hal) (Jun. 2018) 95–104, https://doi.org/10.1016/j.tsf.2018.04.014.

[11] A. Ashok, et al., Comparative studies of CdS thin films by chemical bath deposition techniques as a buffer layer for solar Cell Applications, J. Mater. Sci. Mater. Electron. 31 (10) (2020) 7499–7518, https://doi.org/10.1007/s10854-020-03024-3.

[12] S. Tobbeche, et al., Improvement of the CIGS solar cell performance: structure based on a ZnS buffer layer, *Opt. Quantum Electron.*, Agu 51 (8) (2019), https://doi.org/10.1007/s11082-019-2000-z, 2019.

[13] C. Ou, et al., Bandgap tunable CdS:O as efficient electron buffer layer for high-performance Sb2Se3 thin film solar cells, Sol. Energy Mater. Sol. Cells 194 (2019) 47–53, https://doi.org/10.1016/j.solmat.2019.01.043. Jun.

[14] J.C. Park, M. Al-Jassim, S.W. Shin, J.H. Kim, dan T.W. Kim, Comprehensive characterization of CIGS absorber layers grown by one-step sputtering process, Ceramics International 45 (4) (2019) 4424–4430, https://doi.org/10.1016/j.ceramint.2018.11.120.

[15] C.-H. Huang, W.-J. Chuang, C.-P. Lin, Y.-L. Jan, dan Y.-C. Shih, Deposition technologies of high-efficiency CIGS solar cells: development of two-step and Co-evaporation processes, Crystals 8 (7) (Jul 2018) 296, https://doi.org/10.3390/cryst8070296.

[16] T. Zhang, et al., High efficiency solution-processed thin-film Cu(In,Ga)(Se,S)2 solar cells, Energy Environ. Sci. 9 (12) (2016) 3674–3681, https://doi.org/10.1039/C6EE02352E.

[17] M. Wang, et al., Effect of sodium treatment on the performance of electrostatic spray assisted vapour deposited copper-poor Cu(in,Ga)(S,Se) 2 solar cells, *Sci. Rep.*, Des 7 (1) (2017) 6788, https://doi.org/10.1038/s41598-017-07027-9. PMID: 28754902.

[18] A.S.P. Dewi, et al., Synthesis and Characterization of CIGS Ink by Hot Injection Method, 2020, https://doi.org/10.1063/5.0000878 hal. 020002..

[19] A.S.P. Dewi, et al., Synthesis and Characterization of CIGS/ZnO Film by Spin Coating Method for Solar Cell Application, 2020, https://doi.org/10.1063/5.0002493, 040064.

[20] Y. Zhang, et al., Silver surface treatment of Cu(in,Ga)Se 2 (CIGS) thin film: a new passivation process for the CdS/CIGS heterojunction interface, Sol. RRL 4 (10) (2020), 2000290, https://doi.org/10.1002/solr.202000290.

[21] C.H. Wu, et al., Effect of Selenization processes on CIGS solar cell performance, J. Nanosci. Nanotechnol. 18 (7) (Jul. 2018) 5074–5081, https://doi.org/10.1166/jnn.2018.15279. PMID:29442696.

[22] M.-T. Sun, et al., Effects of selenization process on densification and microstructure of Cu(In,Ga)Se2 thin film prepared by doctor blading of CIGS nanoparticles, Ceram. Int. 44 (16) (2018) 20508–20513, https://doi.org/10.1016/j.ceramint.2018.08.047.

[23] B.S. Yadav, et al., Microstructural investigation of inkjet printed Cu(In,Ga)Se2 thin film solar cell with improved efficiency, J. Alloys Compd. 827 (2020), 154295, https://doi.org/10.1016/j.jallcom.2020.154295. Jun.

[24] K. Madhuri, P.K. Kannan, B.S. Yadav, S. Chaudhari, S.R. Dhage, dan S.R. Dey, Investigation on effects of precursor pre-heat treatments on CIGS formation using spin-coated CIG precursor, J Mater Sci: Mater Electron 32 (2) (2021) 1521–1527, https://doi.org/10.1007/s10854-020-04921-3. Jan.

[25] C.-H. Huang dan, D.-C. Wen, The effects of annealing parameters on the crystallization and morphology of Cu(in,Ga)Se 2 absorber layers prepared by annealing stacked metallic precursors, Int. J. Photoenergy (2014) 1–8, https://doi.org/10.1155/2014/568648.

[26] Y. Lv, et al., Separation and recovery of valuable elements from spent CIGS materials, *ACS Sustain. Chem. Eng.*, Des 2019 7 (24) (2019) 19816–19823, https://doi.org/10.1021/acssuschemeng.9b05121.

[27] E. Zhao, et al., In situ fabrication of 2D SnS2 nanosheets as a new electron transport layer for perovskite solar cells, Nano Res 11 (11) (2018) 5913–5923, https://doi.org/10.1007/s12274-018-2103-z.

[28] E. Ghanbari, et al., Improving CIGS thin film by evaporation of CIGS nanoparticles without phase change, Appl. Phys. A 125 (5) (2019), https://doi.org/10.1007/s00339-019-2561-5.

[29] P.C. Huang, et al., Effect of selenization and sulfurization on the structure and performance of CIGS solar cell, J. Mater. Sci. Mater. Electron. 29 (2) (2018) 1444–1450, https://doi.org/10.1007/s10854-017-8052-6. Jan.

[30] N. Khoshsirat, et al., Analysis of absorber layer properties effect on CIGS solar cell performance using SCAPS, Optik 126 (7–8) (Apr. 2015) 681–686, https://doi.org/10.1016/j.ijleo.2015.02.037.

[31] F. Najafkhani, et al., Recent advances in the kinetics of normal/abnormal grain growth: a review, Arch. Civ. Mech. Eng. 21 (1) (2021), https://doi.org/10.1007/s43452-021-00185-8.

[32] M.I. Khan, et al., Entropy generation minimization and binary chemical reaction with Arrhenius activation energy in MHD radiative flow of nanomaterial, J. Mol. Liq. 259 (Jun. 2018) 274–283, https://doi.org/10.1016/j.molliq.2018.03.049, hal.

[33] Z.A. Piskulich, et al., Activation energies and beyond, *J. Phys. Chem. A*, Agu 123 (33) (2019) 7185–7194, https://doi.org/10.1021/acs.jpca.9b03967. PMID: 31250645.

[34] J. Bi, et al., Three-step vapor Se/N2/vapor Se reaction of electrodeposited Cu/In/Ga precursor for preparing CuInGaSe2 thin films, Sol. Energy Mater. Sol. Cells 159 (Jan. 2017) 352–361, https://doi.org/10.1016/j.solmat.2016.09.026, hal.

[35] S.C. Chen, et al., A comprehensive study of one-step Selenization process for Cu (In1−x Ga x)Se2 thin film solar cells, *Nanoscale Res. Lett.*, Des 12 (1) (2017) 208, https://doi.org/10.1186/s11671-017-1993-0. PMID:28330186.

[36] M. Abdullah dan Khairurrijal, 194-ArticleText-635-1-10-20161103.pdf, Indonesian J. Phys., 2009.

[37] Y.C. Lin, et al., Cu(In,Ga)Se2 films prepared by sputtering with a chalcopyrite Cu (In,Ga)Se2 quaternary alloy and in targets, J. Mater. Sci. Mater. Electron. 23 (2) (2012) 493–500, https://doi.org/10.1007/s10854-011-0424-8.

[38] T. Dzhafarov dan, A. Bayramov, Porous silicon and solar cells, in: L. Canham (Ed.), Handbook of Porous Silicon, Springer International Publishing, Cham, 2017, pp. 1–14, https://doi.org/10.1007/978-3-319-04508-5_95-2.

[39] L. Choubrac, et al., Cu(In,Ga)Se 2 solar cells with improved current based on surface treated stoichiometric absorbers, Phys. Status Solidi (A) 214 (1) (Jan. 2017), 1600482, https://doi.org/10.1002/pssa.201600482.

[40] F. Ahmad, et al., Efficiency enhancement of ultrathin CIGS solar cells by optimal bandgap grading, *Appl. Opt.*, Agu 2019 58 (22) (2019) 6067–6078, https://doi.org/10.1364/AO.58.006067. PMID:31503927.

[41] A. Sylla, et al., Numerical modeling and simulation of CIGS-based solar cells with ZnS buffer layer, Open J. Modell. Simul. 5 (4) (2017) 218–231, https://doi.org/10.4236/ojmsi.2017.54016.

[42] M. Wang, et al., Electrodeposition of Mg doped ZnO thin film for the window layer of CIGS solar cell, Appl. Surf. Sci. 382 (Sep. 2016) 217–224, https://doi.org/10.1016/j.apsusc.2016.03.232.

[43] A.C. Badgujar, R.O. Dusane, dan S.R. Dhage, Cu(In,Ga)Se2 thin film absorber layer by flash light post-treatment, Vacuum 153 (Jul 2018) 191–194, https://doi.org/10.1016/j.vacuum.2018.04.021.

[44] F. Konstantinos, Modeling and Simulation of a Dual-Junction CIGS Solar Cell Using Silvaco ATLAS, Naval Postgraduate School, 2012. T. Pada. Available at: https://core.ac.uk/download/pdf/36720661.pdf.

[45] A.C. Badgujar, R.O. Dusane, dan S.R. Dhage, Cu(In,Ga)Se2 thin film solar cells produced by atmospheric selenization of spray casted nanocrystalline layers, Solar Energy 209 (2020) 1–10, https://doi.org/10.1016/j.solener.2020.08.080.

[46] P. Paul, et al., in: Impact of the Ga/In Ratio on Defects in Cu(In,Ga)Se2, IEEE, 2016 [Daring]. T. Pada. Available at: https://ieeexplore.ieee.org/abstract/document/7750035.

[47] A.C. Badgujar, R.O. Dusane, dan S.R. Dhage, Pulsed laser annealing of spray casted Cu(In,Ga)Se2 nanocrystal thin films for solar cell application, Solar Energy 199 (2020) 47–54, https://doi.org/10.1016/j.solener.2020.02.023.7.